NONLINEAR CONTROL DESIGN FOR MAXIMUM POWER POINT TRACKING OF A PMSG-BASED WIND TURBINE

Saleh Alshamali[1], Dana Alawadhi[2] and Elham Aljuwaiser[1]

[1]Electrical Engineering Department
College of Engineering and Petroleum
Kuwait University
P. O. Box 5969, Safat 13060, Kuwait
{ s.alshamali; eng.elham }@ku.edu.kw

[2]Engineering and Maintenance Department
Public Authority of Applied Education and Training
P. O. Box 23778, Safat 22081, Kuwait
dn.alawadhi@paaet.edu.kw

ABSTRACT. *This paper deals with the design of nonlinear controllers for a variable speed permanent magnet synchronous generator (PMSG)-based wind turbine. In particular, the design seeks to maximize the generated power of a wind turbine operating in Region II where the wind speed is below the rated wind speed. The control design uses the maximum power point tracking (MPPT) method to maximize energy extraction. The key step in the design is the introduction of a state transformation that renders the nonlinear dynamics of the wind turbine system into a form that is suitable for a variety of control designs. Two control design schemes, a feedback linearization control and a sliding mode control (SMC), are then proposed to achieve maximum power point tracking. It is shown that the proposed controllers guarantee the asymptotic convergence of all state trajectories to their desired values, and guarantee maximum power tracking. The stability of the closed-loop system is proven through Lyapunov stability theory, and the effectiveness of the nonlinear controllers is demonstrated through simulation studies.*
Keywords: Nonlinear control, Control applications, Wind energy system, Permanent magnet synchronous generator, MPPT, Feedback linearization, Sliding mode control

1. **Introduction.** In recent years, governments have become increasingly aware of the importance of renewable energy. As a result, they are investing in the development of major sources of renewable energy, such as wind, solar, and hydroelectric energy. Wind turbines play a significant role in capturing wind energy and converting it into electrical power. Maximum power point tracking (MPPT) technology is used to maximize power generation at wind speeds below the rated wind speed [1]. In the literature, several studies have focused on control applications in wind turbine systems. The research below summarizes a selection of the many control techniques that have been employed.

The work in [2] presented a new method for voltage regulation in microgrids. The authors developed a large-signal model based on the concept of virtual synchronous generators (VSGs). The system's voltage is then regulated using feedback linearization and LQR methods. The suggested technique has been proven to be successful in regulating the voltage while providing inertia and damping for microgrids. In [3], a super-twisting sliding mode control (SMC) was proposed for the generator and the grid-side converter to regulate the DC-link voltage of a permanent magnet synchronous generator (PMSG)

wind turbine. The proposed controller was shown to be effective in achieving MPPT under grid fault conditions. A control design based on first- and higher-order SMC for a PMSG wind turbine system with bounded parameter variations was presented in [4]. The controller was shown to be robust against bounded parameter variations. A modified perturb and observe algorithm for optimizing power extraction from PMSG wind turbine systems was introduced in [5]. The suggested approach improves the efficiency of small scale stand-alone wind turbine systems by altering the duty cycle of the buck converter without the need for a mechanical sensor. Experimental results have shown that the proposed strategy produces satisfactory results. In [6], a combined backstepping control law and model predictive control (MPC) was used for the reliable operation of a PMSG-based wind turbine under normal and grid fault conditions. While the backstepping control is designed in continuous time to stabilize the dynamics, the MPC is designed for the discretized system to track the state reference signals. An improved maximum power point tracking algorithm for a direct-driven wind turbine was proposed in [7]. The algorithm creates a DC voltage reference signal, and then, a nonlinear control is designed to track the desired reference. In [8], a polynomial disturbance observer was constructed for a wind energy conversion system (WECS). The proposed observer estimates the electromagnetic torque, aerodynamic torque, wind speed, and disturbances. A linear quadratic regulator (LQR) then uses these estimates to reject disturbances and achieve MPPT. In [9], the control problem of a wind turbine with a doubly fed induction generator (DFIG) was examined. Vector control was utilized to track the maximum power point in the region when wind speeds were less than the rated wind speed. For wind speeds greater than the specified wind speed, a PI controller based on Taylor linearization was used to manage the pitch dynamics. The MPPT algorithm, along with the pitch control, was shown to give good performance. An integral backstepping control law was proposed in [10] to attain the MPPT for a wind energy system based on a PMSG. The proposed controller's performance was compared to that of the sliding mode controller. The energy generated by the PMSG under the integrated backstepping controller was found to be of higher quality than that generated by the sliding mode controller. To compensate for the lag in wind speed measurement, a bat algorithm is employed in [11] to improve an extreme learning machine (ELM) to anticipate wind speed. Then, using the forecasted wind speed, a state-feedback control law is designed to accomplish MPPT. In [12], the control of a variable-speed squirrel-cage induction generator (SCIG)-based wind turbine using an SMC scheme was presented. One controller is used to achieve MPPT, whereas the other controls the grid-side converter, which regulates the DC-link voltage. The study in [13] proposed a model reference adaptive control (MRAC) for a small wind turbine with a PMSG to maximize power extraction in Region II. A state feedback control utilizing the forecasted values is then used to achieve MPPT. The work in [14] provided a novel structure for small-scale wind turbine systems as well as an MPPT-Fuzzy controller architecture for improved quality control. The suggested controller provides advantages such as fast response and flexibility. It was demonstrated that the recommended controller outperformed the typical controller based on hill climb search. In [15], a sliding mode control observer based on the supertwisting algorithm was presented to estimate aerodynamic torque and rotor acceleration. Then, SMC was developed for the torque and pitch control of a wind turbine system with a PMSG. The proposed control scheme was shown to be robust against wind turbulence. In [16], a nonlinear backstepping controller, incorporating a high gain term, was designed for a PMSG-based wind turbine system. The controller is aimed at tracking a desired rotation speed under unknown wind torque dynamics. The proposed control scheme was found to have a faster response and more

precise tracking than the typical vector control technique. A back-to-back (BTB) converter of a PMSG-based wind turbine was controlled through a PID-type terminal SMC [17]. The controller was able to stabilize the machine side as well as the grid side of the BTB converter despite the voltage variations in the DC-link. In [18], an MPPT algorithm based on the voltage-power (U-P) curve was proposed for a small wind turbine without the need for wind speed or mechanical rotor speed measurement. The rotor speed was estimated using the voltage-current information from the generator. The proposed technique outperformed methods based on the (ω-P) curve. The stabilization of a wind energy system under parametric uncertainties through integral terminal sliding mode control (ITSMC) was addressed in [19]. The proposed controller was shown to regulate the converters on the generator side and grid side while overcoming uncertainties.

This study aims to design nonlinear controllers for a variable-speed wind turbine equipped with a permanent-magnet synchronous generator to maximize the generated power in Region II. The main contributions of this study are as follows. First, a state transformation that transforms the nonlinear dynamics of the wind turbine system into a canonical form, which facilitates the subsequent control design, is introduced. The transformation that is being suggested brings the dynamics of the wind turbine system into a normal form, which makes it possible to use a wide variety of control design strategies. Subsequently, a feedback linearization control law and an SMC are designed to steer the state trajectories to their desired values. Finally, a robust SMC scheme is proposed for a wind turbine system subject to external disturbances.

The remaining sections of the paper are structured as follows. The development of the PMSG-based wind turbine model is presented in Section 2. Section 3 presents a transformation that maps the nonlinear dynamics into a form that eases the control design. The employment of a feedback linearizing controller for the transformed system is presented in Section 4. Section 5 demonstrates the design of a sliding mode control for the transformed wind turbine system. In Section 6, a robust SMC is proposed for a wind turbine system under external disturbance. Simulation studies demonstrating the effectiveness of the proposed controllers are presented in Section 7, followed by concluding remarks in Section 8.

2. **Model of the Wind Turbine System.**

2.1. **The aerodynamic model.** Wind turbines do not capture all wind energy. The aerodynamic power (output power) of the wind turbine is given by

$$P_w = \frac{1}{2}\rho A C_p(\lambda, \beta) v^3$$

where ρ: the air density; A: the area swept by the blades of the turbine [m^2]; $C_p(\lambda, \beta)$: the coefficient of power conversion; λ: the tip speed ratio [m/s]; β: the blade pitch angle; v: the wind speed [m/s].

It is assumed that the wind speed is a smooth function of time. Figure 1 depicts the dependence of the power coefficient C_p on the blade angle β (in degrees) and the tip speed ratio λ. It can be observed from the figure that the power coefficient is maximum when $\beta = 0$. The power coefficient describes the efficiency of the power extraction. A typical function of the power coefficient C_p is given by [19]

$$C_p(\lambda, \beta) = c_1 \left(\frac{c_2}{\Gamma} - c_3\beta - c_4 \right) e^{-\frac{c_5}{\Gamma}} \tag{1}$$

where Γ is defined as

$$\frac{1}{\Gamma} = \frac{1}{\lambda + c_6\beta} - \frac{c_7}{1 + \beta^3} \tag{2}$$

and the constant coefficients $c_1, \ldots, c_7$ depend on the type of the wind turbine rotor. The tip speed ratio λ is related to the wind speed v by

$$\lambda = \frac{\omega_m r}{v} \tag{3}$$

where ω_m is the mechanical rotor speed of the turbine [rad/s], and r is the radius of the rotor [m]. The mechanical torque [N.m] that is transmitted to the generator is given by

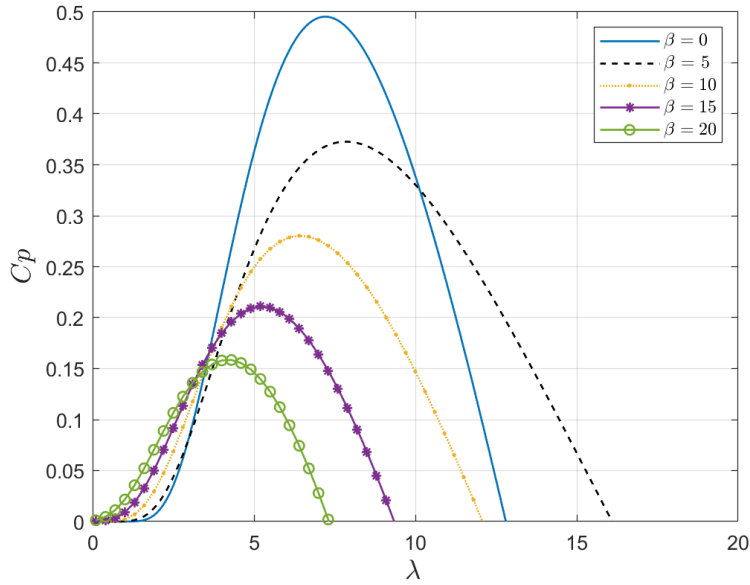$$T_m = \frac{P_w}{\omega_m} = \frac{0.5 \rho A C_p(\lambda, \beta) v^3}{\omega_m}$$

FIGURE 1. Wind turbine power coefficient

2.2. **The generator model.** The mathematical model of the PMSG in the d-q reference frame is derived from the equivalent circuits shown in Figures 2 and 3.
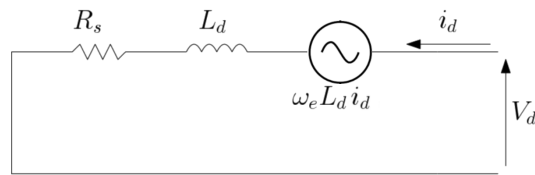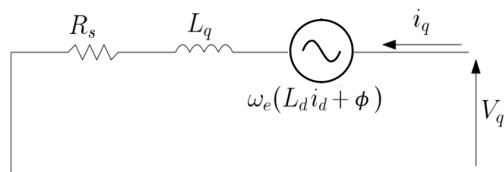

FIGURE 2. The d-axis equivalent circuit

FIGURE 3. The q-axis equivalent circuit

The voltage equations can be expressed as

$$V_d = R_s i_d + \frac{d}{dt} L_d i_d - \omega_e L_q i_q$$

$$V_q = R_s i_q + \frac{d}{dt} L_q i_q - \omega_e (L_d i_d + \phi)$$

where V_d, V_q: the d-q axis voltages [V]; i_d, i_q: the direct and quadrature axis currents [A]; R_s: the stator resistance [Ω]; L_d, L_q: the dq axis inductances [mH]; ϕ: the permanent magnetic flux [Wb]; ω_e: the electrical rotor speed [rad/s].

The electrical rotor speed is related to the mechanical rotor speed by

$$\omega_e = PN\omega_m \tag{4}$$

where P is the number of pole pairs of the generator and N is the gear ratio. In this work, it is assumed that the PMSG has a uniform air gap; therefore, $L_d = L_q = L$. Furthermore, ignoring the viscous friction coefficient of the rotor, the drive train dynamics can be expressed as

$$\frac{d\omega_m}{dt} = \frac{1}{J}(T_m - T_e)$$

where J is the inertia of the turbine, and T_e is the electrical torque. Finally, combining the voltage equations with the drive-train dynamics and using Equation (4), the PMSG model is given by

$$\dot{i}_d = -\frac{R_s}{L} i_d + \omega_e i_q + \frac{1}{L} V_d$$
$$\dot{i}_q = -\frac{R_s}{L} i_q - \omega_e i_d - \frac{\omega_e \phi}{L} + \frac{1}{L} V_q$$
$$\dot{\omega}_e = \frac{P}{J}\left(\frac{T_m}{N} - T_e\right)$$

where the electromagnetic torque T_e is given by

$$T_e = \frac{3}{2} P \phi i_q$$

For convenience, the state vector, $x(t)$, is defined as $x = [x_1 \ x_2 \ x_3]^T = [i_d \ i_q \ \omega_e]^T$, and the control vector $[u_1 \ u_2]^T = [V_d \ V_q]^T$. Furthermore, to simplify the subsequent analysis, the following constant parameters are defined: $a_1 = \frac{R_s}{L}$, $a_2 = \frac{1}{L}$, $a_3 = \frac{\phi}{L}$, $a_4 = \frac{P}{JN}$, and $a_5 = \frac{3P^2\phi}{2J}$. The new dynamics of the PMSG can be expressed as

$$\dot{x}_1 = -a_1 x_1 + x_2 x_3 + a_2 u_1$$
$$\dot{x}_2 = -a_1 x_2 - x_1 x_3 - a_3 x_3 + a_2 u_2$$
$$\dot{x}_3 = a_4 T_m - a_5 x_2 \tag{5}$$

2.3. **The error dynamics.** The error dynamics are obtained in this subsection. To this end, let $e(t) = x(t) - x_d(t)$ be such that

$$e_1 = x_1 - x_{1d}$$
$$e_2 = x_2 - x_{2d}$$
$$e_3 = x_3 - x_{3d}$$

where $x_d(t) = [x_{1d} \ x_{2d} \ x_{3d}]^T$ is the vector of desired, steady-state trajectories, whose dynamics are given by

$$\dot{x}_{1d} = -a_1 x_{1d} + x_{2d} x_{3d} + a_2 u_{1ss}$$
$$\dot{x}_{2d} = -a_1 x_{2d} - x_{1d} x_{3d} - a_3 x_{3d} + a_2 u_{2ss}$$
$$\dot{x}_{3d} = a_4 T_m^* - a_5 x_{2d} \tag{6}$$

where u_{1ss} and u_{2ss} represent the steady-state values of the control signals $u_1(t)$ and $u_2(t)$, respectively, and T_m^* is the mechanical torque at maximum power generation. Taking the time-derivative of the error signals and using Equations (5) and (6), the error dynamics can be expressed as

$$\dot{e}_1 = -a_1e_1 + e_2e_3 + x_{3d}e_2 + x_{2d}e_3 - a_2u_{1ss} + a_2u_1$$
$$\dot{e}_2 = -a_1e_2 - a_3e_3 - e_1e_3 - x_{3d}e_1 - x_{1d}e_3 - a_2u_{2ss} + a_2u_2$$
$$\dot{e}_3 = a_4(T_m - T_m^*) - a_5e_2 \tag{7}$$

The steady-state expressions for the state and control variables are found as follows. First, it is common to set the d-axis current i_d to zero to reduce the copper losses. Therefore, the desired value of the d-axis current is $x_{1d} = 0$. Next, using Equations (3) and (4), the desired value of the electrical rotor speed is given by

$$x_{3d} = PN\omega_m^* = \frac{PN\lambda^*v}{r} \tag{8}$$

where λ^* is the optimum tip speed ratio at which the power coefficient C_p attains its maximum and ω_m^* is the optimal rotor speed. To find the desired value of the q-axis current, x_{2d}, we take the time-derivative of Equation (8) and substitute the result into the $\dot{x}_{3d}$ dynamics in Equation (6). This yields

$$x_{2d} = \frac{a_4}{a_5}T_m^* - \frac{PN\lambda^*}{a_5r}\dot{v} \tag{9}$$

where, from Equation (4), the mechanical torque at the optimum values can be expressed as

$$T_m^* = \frac{QC_p^*(\lambda, \beta)v^3}{x_{3d}}$$

where $Q = 0.5\rho\pi r^2 PN$. Additionally, we have used Equation (4) and the area swept by the turbine blades $A = \pi r^2$. The steady-state expressions for the d-axis and q-axis voltages, u_{1ss} and u_{2ss}, respectively, can be found as follows. First, using $x_{1d} = 0$ from the $\dot{x}_{1d}$ dynamics in Equation (6), the steady-state value of the d-axis voltage can be written as

$$u_{1ss} = -\frac{x_{2d}x_{3d}}{a_2}$$

The expression for u_{2ss} can be obtained by taking the time-derivative of x_{2d} in Equation (9), and substituting the result into the $\dot{x}_{2d}$ dynamics in Equation (6) to obtain

$$u_{2ss} = \frac{1}{a_2}\left(\frac{a_4}{a_5}\dot{T}_m^* - \frac{PN\lambda^*}{a_5r}\ddot{v} + a_1x_{2d} + a_3x_{3d}\right)$$

3. **State Transformation.** From dynamic Equation (7), it can be observed that with an appropriate choice for the control signals $u_1(t)$ and $u_2(t)$, the errors e_1 and e_2 can be driven to zero at $t \to \infty$. However, the error signal e_3, and therefore the state variable $x_3(t)$ cannot be affected by the control signals. Therefore, we introduce a transformation that transforms the error dynamics model into a companion form such that a variety of control schemes can be applied. Furthermore, as the subsequent analysis shows, all error signals can be driven to zero. To this end, we define the transformation $z = T(e)$ as follows:

$$z_1 = e_1$$
$$z_2 = e_3$$
$$z_3 = a_4(T_m - T_m^*) - a_5e_2 \tag{10}$$

It can be observed that transformation (10) is a diffeomorphism. Taking the time-derivative of the state vector $z(t)$, and with the choice of the control signals,

$$u_1 = \frac{1}{a_2}\left(a_1 e_1 - e_2 e_3 - x_{3d} e_2 - x_{2d} e_3 + a_2 u_{1ss} + e_3\right)$$

$$u_2 = \frac{1}{a_2}\left(a_1 e_2 + a_3 e_3 + e_1 e_3 + x_{3d} e_1 + a_2 u_{2ss} - u(t)\right)$$

where $u(t)$ is an auxiliary control variable, the dynamics of the transformed system become

$$\dot{z}_1 = z_2$$
$$\dot{z}_2 = z_3$$
$$\dot{z}_3 = f + a_5 u \tag{11}$$

where $f = a_4\left(\dot{T}_m - \dot{T}_m^*\right)$, and

$$\dot{T}_m = \frac{\partial T_m}{\partial \omega_e}\dot{\omega}_e + \frac{\partial T_m}{\partial \beta}\dot{\beta} + \frac{\partial T_m}{\partial v}\dot{v} \tag{12}$$

Now, due to the fact that $\beta = 0$ in Region II, expression (2) reduces to

$$\frac{1}{\Gamma} = \frac{1}{\lambda} - c_7 \tag{13}$$

Also, substituting Equation (4) into Equation (3), the tip speed ratio can be expressed as

$$\lambda = \frac{\omega_e r}{PNv} \tag{14}$$

Furthermore, from Equation (14) and Equation (13), expression (1) for the function of the power coefficient can be written as

$$C_p\left(\omega_e, v\right) = c_1\left(\frac{c_2 PNv}{\omega_e r} - c_2 c_7 - c_4\right) e^{-c_5\left(\frac{PNv}{\omega_e r} - c_7\right)} \tag{15}$$

Finally, using Equation (15) and the fact that $T_m = \left(Qv^3/\omega_e\right)C_p(\omega_e, v)$, expression (12) can be written as

$$\dot{T}_m = \left(-Qv^3 C_p \frac{1}{\omega_e^2} + \frac{Qv^3}{\omega_e}\frac{\partial C_p}{\partial \omega_e}\right)\dot{\omega}_e + \left(\frac{3Qv^2 C_p}{\omega_e} + \frac{Qv^3}{\omega_e}\frac{\partial C_p}{\partial v}\right)\dot{v}$$

4. **Design of a Feedback Linearization Controller.** In this section, a control design based on the feedback linearization methodology is proposed for the wind turbine system. Note that transforming the wind turbine dynamics into the normal form given by (11) makes feedback linearization design straightforward. The following propositions present the main results.

Proposition 4.1. *The nonlinear dynamics of the wind turbine system in (5) are asymptotically stable under the feedback linearizing controller:*

$$u(t) = -\frac{1}{a_5}\left(a_4\left(\dot{T}_m - \dot{T}_m^*\right) + \alpha_1 z_1 + \alpha_2 z_2 + \alpha_3 z_3\right) \tag{16}$$

where α_1, α_2, and α_3 are positive scalars to be designed.

Proof: We consider the dynamics of the transformed system (11). By substituting for the control law in (16), the dynamics of the closed-loop system are expressed as

$$\dot{z}(t) = A_{c1} z(t)$$

where A_{c1} is given by

$$A_{c1} = \begin{bmatrix} 0 & 1 & 0 \\ 0 & 0 & 1 \\ -\alpha_1 & -\alpha_2 & -\alpha_3 \end{bmatrix}$$

With an appropriate choice of the parameters α_i $(i = 1, 2, 3)$, the eigenvalues of the closed-loop matrix A_{c1} can be placed in the left-half plane, thus ensuring the asymptotic stability of the transformed system dynamics such that $z_i(t)$ $(i = 1, 2, 3)$ converge to the origin as t tends to infinity.

From transformation (10), because $z_1, z_2 \to 0$ as $t \to \infty$, then $e_1, e_3 \to 0$ as $t \to \infty$. Therefore, both the d-axis current, x_1, and the electrical rotor speed, x_3, converge to their desired values, x_{1d} and x_{3d}. Furthermore, because $z_3 \to 0$ as $t \to \infty$, then $e_2 \to \frac{a_4}{a_5}(T_m - T_m^*)$. Now, from the expression of T_m (T_m^*), because the wind speed, v, is bounded, and because it was established that $x_3 \to x_{3d}$ (or $\omega_e \to \omega_e^*$), then we can show that $e_2 \to 0$ if maximum power tracking is attained. Considering Region II $(\beta = 0)$, from the expression of the tip speed ratio, λ, in Equation (3), it was shown that $\omega_e \to \omega_e^*$ (or $\omega_m \to \omega_m^*$). Thus, $\lambda \to \lambda^*$ and as a consequence $C_p(\lambda, \beta)$ attains its maximum value. Finally, we can conclude that $e_2 \to 0$ as $t \to \infty$, that is, the q-axis current, x_2, converges to its desired value x_{2d} as $t \to \infty$.

5. **Sliding Mode Control Design.** This section develops a nonlinear controller for a wind turbine system using the SMC approach. SMC is a control strategy that is well known for its fast response and robustness against parameter uncertainties and external disturbances. It consists of a reaching phase, where the state trajectories are forced towards a predefined manifold (also known as a sliding surface), and a sliding phase, where the state trajectories are forced to stay on the manifold once it is reached [20].

The derivation of the SMC is based on the following proposed sliding surface σ:

$$\sigma(t) = z_3 + k_1 z_1 + k_2 z_2 \tag{17}$$

where k_1 and k_2 are positive scalars chosen such that the polynomial $P(s) = s^2 + k_2 s^3 + k_1$ is Hurwitz. The advantage of using a linear sliding manifold is that the closed-loop dynamics are of reduced order.

Proposition 5.1. *The nonlinear dynamics of the wind turbine system in (5) are asymptotically stable under the sliding mode controller:*

$$u(t) = -\frac{1}{a_5}\left(a_4\left(\dot{T}_m - \dot{T}_m^*\right) + k_1 z_2 + k_2 z_3 + \eta\sigma + W\,sign(\sigma)\right) \tag{18}$$

where $\eta, W > 0$ are scalars to be designed.

Proof: To ensure finite time convergence to the sliding manifold, the reachability condition, that is, $\sigma\dot{\sigma} < 0$, must be satisfied. This condition ensures that the sliding surface is attractive so that the trajectories are driven towards the sliding manifold.

To this end, select the Lyapunov function candidate $V(t)$ such that

$$V = \frac{1}{2}\sigma^2$$

Taking the time-derivative of $V(t)$ along the trajectories of (11) and substituting for the control law in (18), it follows that

$$\dot{V}(t) = \sigma\dot{\sigma}$$
$$= \sigma\{\dot{z}_3 + k_1\dot{z}_1 + k_2\dot{z}_2\}$$
$$= \sigma\{f + a_5 u + k_1 z_2 + k_2 z_3\}$$

$$= \sigma \left\{ f + k_1 z_2 + k_2 z_3 - \left(a_4 \left(\dot{T}_m - \dot{T}_m^* \right) + k_1 z_2 + k_2 z_3 + \eta \sigma + W sign(\sigma) \right) \right\}$$
$$= -\eta |\sigma|^2 - W|\sigma|$$

Because η and W are positive scalars, it follows that $\dot{V}$ is negative definite when $\sigma \neq 0$. Consequently, the sliding manifold is attained in finite time. From Equation (17), once the sliding manifold is reached, then $\sigma = 0$ such that $z_3 = -k_1 z_1 - k_2 z_2$. Thus, the closed-loop dynamics can be expressed as

$$\dot{\bar{z}} = A_{cl} \bar{z}$$

where $\bar{z} = [z_1 \ z_2]^T$, and

$$A_{cl} = \begin{bmatrix} 0 & 1 \\ -k_1 & -k_2 \end{bmatrix}$$

With the appropriate choice of the gain parameters k_1 and k_2, the eigenvalues of the matrix A_{cl} can be placed in the left-half plane, thereby ensuring the asymptotic stability of the closed loop. Because $z_1, z_2 \to 0$ as $t \to \infty$, then $z_3 \to 0$ as $t \to \infty$. Furthermore, from the transformation (10), because $z_1, z_2 \to 0$ as $t \to \infty$, then $e_1, e_3 \to 0$ as $t \to \infty$. The remainder of the proof follows steps similar to those in Section 4. Hence, the state trajectories x_1, x_2, x_3 tend toward their desired values as t tends to infinity.

6. **Robust Sliding Mode Control Design.** In this section, a robust SMC is designed for a wind turbine system under a time-varying external disturbance as follows:

$$\dot{x}_1 = -a_1 x_1 + x_2 x_3 + a_2 u_1$$
$$\dot{x}_2 = -a_1 x_2 - x_1 x_3 - a_3 x_3 + a_2 u_2 + d(t)$$
$$\dot{x}_3 = a_4 T_m - a_5 x_2$$

where the disturbance $d(t)$ is bounded as follows:

$$|d(t)| \leq M \quad (19)$$

where $M > 0$ is a constant. After obtaining the error dynamics and invoking the transformation (10), the transformed system dynamics are given by

$$\dot{z}_1 = z_2$$
$$\dot{z}_2 = z_3$$
$$\dot{z}_3 = f + a_5 u - a_5 d(t) \quad (20)$$

Proposition 6.1. *The nonlinear dynamics of the wind turbine system in (19) are asymptotically stable under the robust sliding mode controller:*

$$u(t) = -\frac{1}{a_5} \left(a_4 \left(\dot{T}_m - \dot{T}_m^* \right) + k_1 z_2 + k_2 z_3 + \eta \sigma + W sign(\sigma) \right) \quad (21)$$

where $\eta > 0$ and $W > |a_5 M|$ are scalars to be designed.

Proof: Consider the sliding surface $\sigma(t) = z_3 + k_1 z_1 + k_2 z_2$, and the Lyapunov function candidate $V(t)$ such that

$$V = \frac{1}{2}\sigma^2$$

Taking the time-derivative of $V(t)$ along the trajectories of (20) gives

$$\dot{V}(t) = \sigma \dot{\sigma} = \sigma \{ f + a_5 u - a_5 d(t) + k_1 z_2 + k_2 z_3 \}$$

Substituting for the control law in (21), it follows that

$$\dot{V}(t) = \sigma \{-\eta\sigma - W sign(\sigma) - a_5 d(t)\}$$

Using the bound on the disturbance in (19), we have

$$\dot{V}(t) \le -\eta|\sigma|^2 - W|\sigma| + |a_5 M||\sigma|$$

Choose $W = |a_5 M| + \zeta$, where $\zeta > 0$, then

$$\dot{V}(t) = -\eta|\sigma|^2 - \zeta|\sigma|$$

Since $\dot{V}(t) < 0$, then finite time convergence is guaranteed. The rest of the proof follows similar steps to those in the previous section.

7. **Results and Discussions.** Simulation studies are presented in this section to demonstrate the usefulness of the suggested controllers in attaining maximum power tracking. The nominal parameters of the PMSG-based wind turbine model are listed in Table 1 [4]. The parameters of the power coefficient function in Equations (1) and (2) c_i $(i = 1, \ldots, 7)$ are such that $c_1 = 0.39$, $c_2 = 116$, $c_3 = 0.4$, $c_4 = 5$, $c_5 = 16.5$, $c_6 = 0.089$, and $c_7 = 0.035$. The maximum power coefficient is $C_p^* = 0.4953$. The wind speed profile is shown in Figure 4.

First, we discuss the simulation results obtained using the feedback linearization controller (16). The controller gains were chosen such that $\alpha_1 = 30$, $\alpha_2 = 29$, $\alpha_3 = 10$. Hence, the eigenvalues of the closed-loop matrix A_{c1} are $\lambda_1 = -6$, and $\lambda_{2,3} = -2 \pm j1$. Figure 5

TABLE 1. Parameters of the wind turbine model

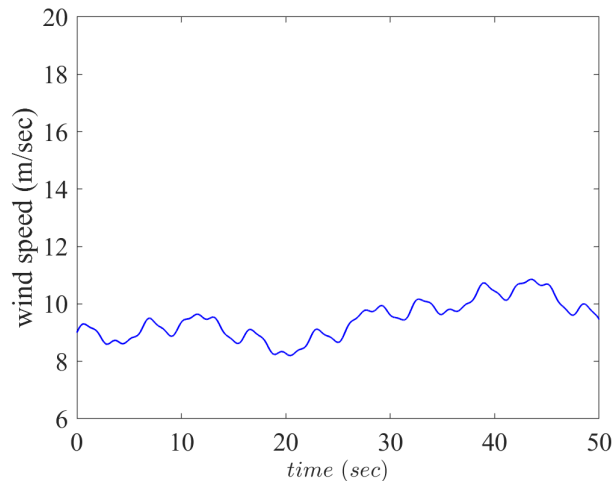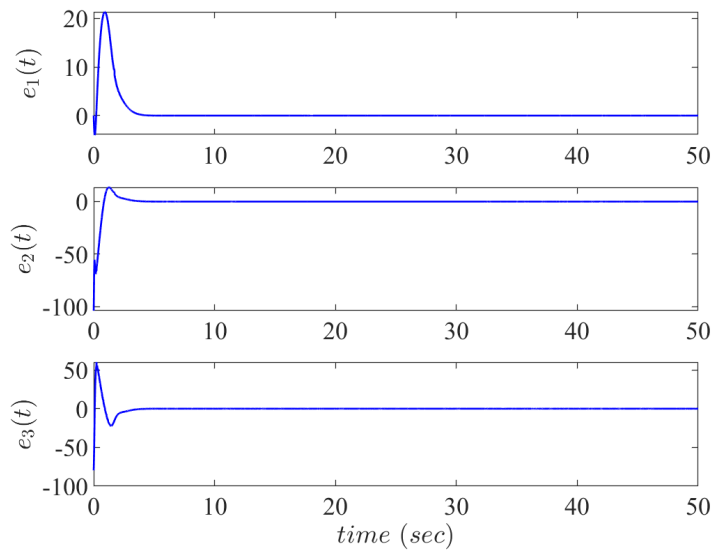| Parameter	Description	Value
r	Radius of the rotor [m]	3
R_s	Stator resistance [Ω]	3.5
L	dq axis inductance [mH]	35
ρ	Air density [kg/m^3]	1.25
ϕ	Permanent magnet flux [Wb]	0.3
P	Number of pole pairs	6
J	Inertia of the turbine [kg·m^2]	1

FIGURE 4. The wind speed profile

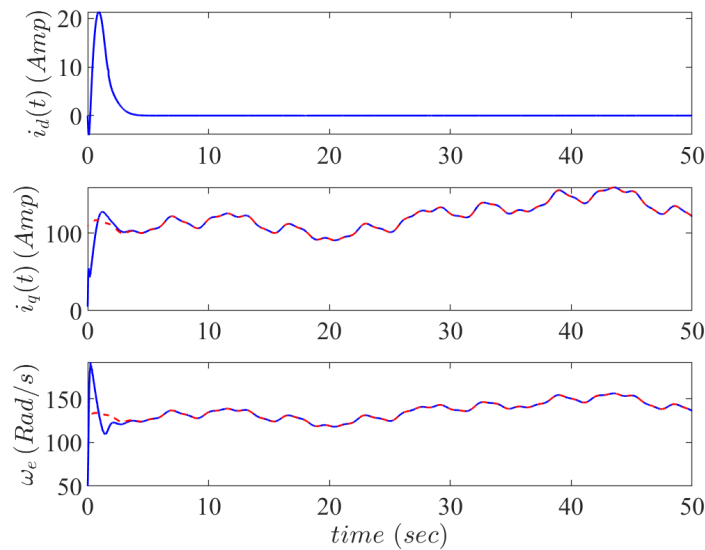FIGURE 5. Error signals under the feedback linearization controller

FIGURE 6. Wind turbine's state trajectories (solid line) vs desired trajectories (dash-dot line) under the feedback linearization controller

shows the asymptotic convergence of the error signals to zero as t tends to infinity. The convergence of the state trajectories towards their desired values is depicted in Figure 6, where the solid line represents the actual states, and the dash-dot line represents the desired values. The control actions of inputs $u_1(t) = V_d$ and $u_2(t) = V_q$ are shown in Figure 7. Finally, Figure 8 shows that the power coefficient attains its maximum value, which demonstrates the effectiveness of the feedback linearizing controller.

Next, we present the simulation results for the developed sliding mode controller given in Equation (18). The controller gains were chosen such that $\eta = 18$ and $W = 2$. The gains of the sliding function, $\sigma(t)$, were chosen as $k_1 = 5$ and $k_2 = 4$ so that closed-loop matrix of the reduced-order dynamics, A_{cl}, is stable with eigenvalues at $\lambda = -2 \pm j$. To eliminate chattering caused by the sliding mode controller, the simulation employs a saturation function rather than the signum function. Figures 9-12 show the performance
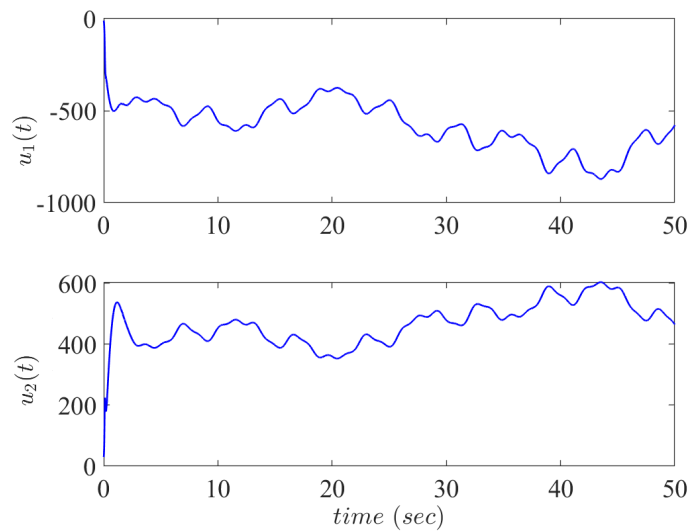
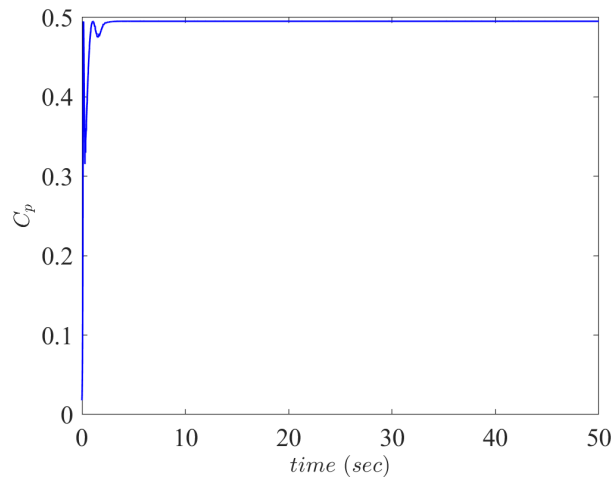FIGURE 7. Direct-axis and quadrature-axis controllers

FIGURE 8. Power coefficient of the wind turbine under the feedback linearization controller

of the sliding mode controller. Figure 9 shows that the error signals tend to zero as time t tends to infinity. The convergence of the state trajectories towards their desired values is depicted in Figure 10, where the solid line represents the actual states, and the dash-dot line represents the desired values. The evolution of the control signals is shown in Figure 11. Figure 12 shows the power coefficient function, C_p, attaining its maximum value of 0.4953, which reveals the effectiveness of the sliding mode controller.

Finally, the robustness of the SMC was demonstrated by considering an uncertain wind turbine model (19). The time-varying bounded disturbance has the form $dt(t) = 0.5\sin(2\pi t)$. The controller gains are chosen as $\eta = 18$ and $W = 9 > |a_5 M|$. It is shown in Figures 13 and 14 that the robust SMC achieves MPPT despite the existence of the external disturbance. In particular, Figure 13 depicts the asymptotic convergence of the state trajectories to their desired values, whereas Figure 14 shows the attainment of the power coefficient function C_p, to its maximum value.

8. **Conclusion.** A control strategy based on feedback linearization and SMC was proposed for tracking the maximum power point in Region II for a PMSG-based wind turbine.
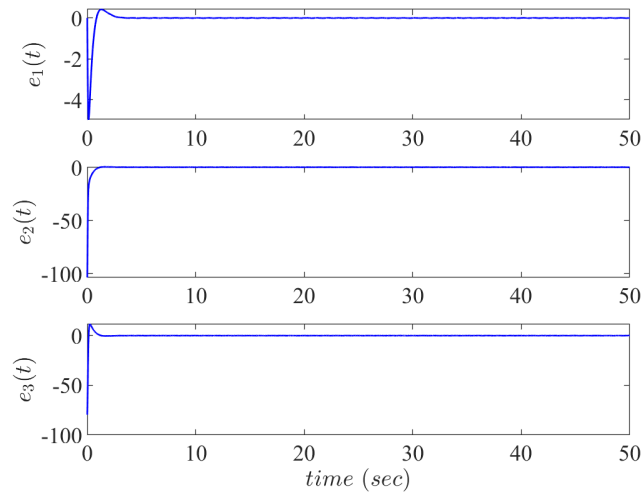
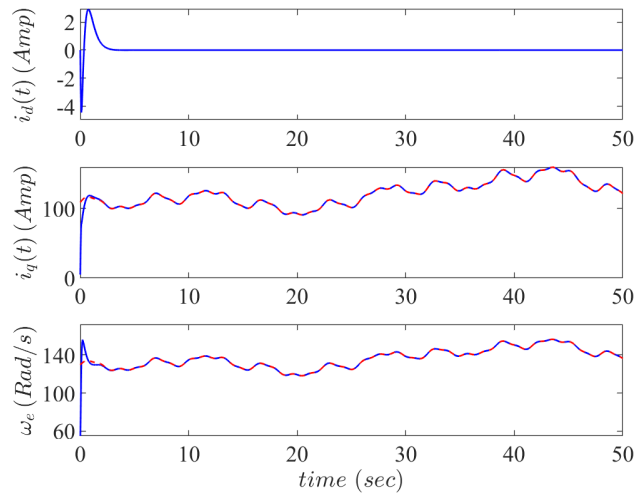FIGURE 9. Error signals under the sliding mode controller

FIGURE 10. Wind turbine's state trajectories (solid line) vs desired trajectories (dash-dot line) under the sliding mode controller
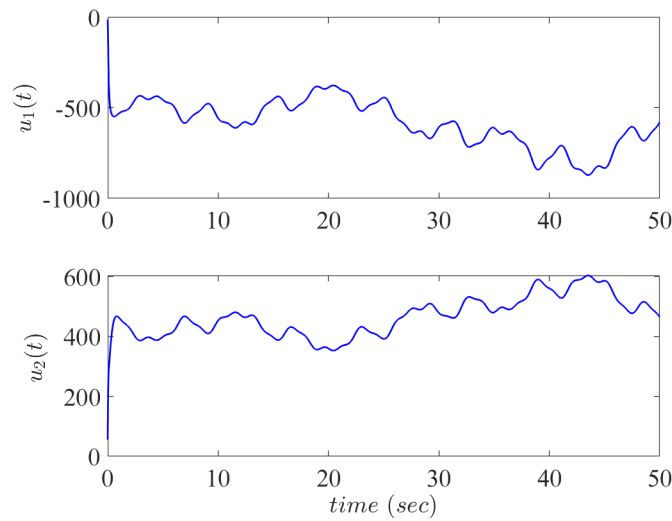

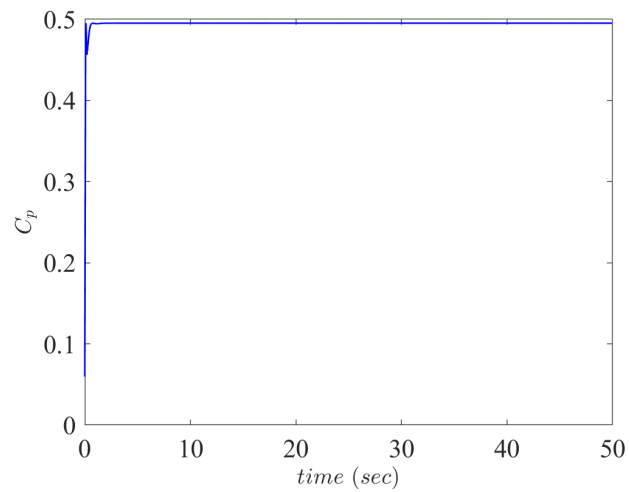FIGURE 11. Direct-axis and quadrature-axis controllers

FIGURE 12. Power coefficient of the wind turbine under the sliding mode controller
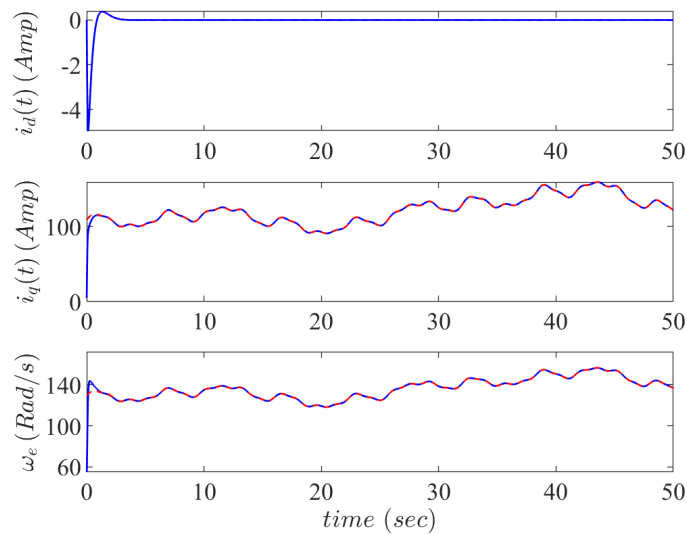

FIGURE 13. Wind turbine's state trajectories (solid line) vs desired trajectories (dash-dot line) under the robust sliding mode controller
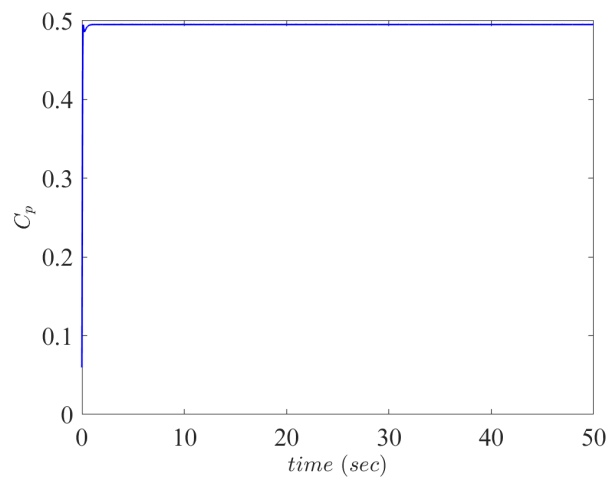

FIGURE 14. Power coefficient of the wind turbine under the robust sliding mode controller

The control design procedure is facilitated by a nonlinear transformation that converts the wind turbine system's nonlinear dynamics into a normal form. The suggested transformation enables the implementation of a wide range of control design techniques. The proposed controllers have been shown to successfully achieve MPPT and drive system trajectories toward their desired values. Furthermore, the robust SMC has been shown to be effective in rejecting time-varying disturbances. The simulation outcomes validate the efficiency of the proposed nonlinear controllers. One limitation of the design is that it is based on the assumption that all states are measurable. Furthermore, the presence of the signum function in the SMC limits its practical implementation. This limitation, however, can be overcome by using an approximation to the signum function. Future work will focus on integrating an observer into the control design to estimate unmeasurable states.

REFERENCES

[1] R. Syahputra and I. Soesanti, Performance improvement for small-scale wind turbine system based on maximum power point tracking control, *Energies*, vol.12, no.20, 3938, 2019.

[2] D. Xu, Z. Cheng, W. Yang and W. Zhang, Robust nonlinear control for virtual synchronous generator based on exact feedback linearization, *International Journal of Innovative Computing, Information and Control*, vol.18, no.4, pp.1133-1145, 2022.

[3] M. Nasiri, S. Mobayen and Q. M. Zhu, Super-twisting sliding mode control for gearless PMSG-based wind turbine, *Complexity*, pp.1-15, 2019.

[4] G. Zhuo, J. D. Hostettler, P. Gu and X. Wang, Robust sliding mode control of permanent magnet synchronous generator-based wind energy conversion systems, *Sustainability*, vol.8, no.12, 1265, 2016.

[5] R. I. Putri, I. N. Syamsiana and M. Rifa'i, Power extraction optimization of PMSG wind turbine system based on simple modified perturb & observe, *ICIC Express Letters, Part B: Applications*, vol.11, no.1, pp.17-24, 2020.

[6] B. Babaghorbani, M. T. Beheshti and H. A. Talebi, A Lyapunov-based model predictive control strategy in a permanent magnet synchronous generator wind turbine, *International Journal of Electrical Power & Energy Systems*, vol.130, 106972, 2021.

[7] A. Dali, S. Abdelmalek, A. Bakdi and M. Bettayeb, A new robust control scheme: Application for MPP tracking of a PMSG-based variable-speed wind turbine, *Renewable Energy*, vol.172, pp.1021-1034, 2021.

[8] V. P. Vu, V. T. Ngo, V. D. Do, D. N. Truong, T. T. Huynh and T. D. Do, Robust MPPT observer-based control system for wind energy conversion system with uncertainties and disturbance, *IEEE Access*, vol.9, pp.96466-96477, 2021.

[9] C. Z. El Archi, T. Nasser, A. Essadki and J. Alvarado, Real power control: MPPT and pitch control in a DFIG based wind turbine, *Proc. of IEEE 3rd International Conference on Advanced Communication Technologies and Networking (CommNet)*, pp.1-6, 2020.

[10] M. Makhad, M. Zazi, A. Loulijat and A. O. Simon, Robust integral backstepping control for optimal power extraction of a PMSG-based variable speed wind turbines, *Proc. of the 1st IEEE International Conference on Innovative Research in Applied Science, Engineering and Technology (IRASET)*, pp.1-6, 2020.

[11] Y. Zhang, L. Zhang and Y. Liu, Implementation of maximum power point tracking based on variable speed forecasting for wind energy systems, *Processes*, vol.7, no.3, 158, 2019.

[12] M. Zribi, M. Alrifai and M. Rayan, Sliding mode control of a variable-speed wind energy conversion system using a squirrel cage induction generator, *Energies*, vol.10, no.5, 604, 2017.

[13] J. Gong and R. Xie, Adaptive control of PMSG-based small wind turbines in Region II, *Proc. of the 35th IEEE Chinese Control Conference (CCC)*, pp.8518-8522, 2016.

[14] N. Quang-Vi, Y. Chai and N. Trong-Thang, The maximum power point tracking based-control system for small-scale wind turbine using fuzzy logic, *International Journal of Electrical and Computer Engineering*, vol.10, pp.3927-3935, 2020.

[15] S. H. Lee, Y. J. Joo, J. H. Back, J. H. Seo and I. Choy, Sliding mode controller for torque and pitch control of PMSG wind power systems, *Journal of Power Electronics*, vol.11, no.3, pp.342-349, 2011.

[16] N. Hawkins and M. L. McIntyre, A robust nonlinear controller for PMSG wind turbines, *Energies*, vol.14, no.4, 954, 2021.

[17] M. Nasiri, S. Mobayen and A. Arzani, PID-type terminal sliding mode control for permanent magnet synchronous generator based enhanced wind energy conversion systems, *CSEE J. Power Energy Syst.*, vol.8, no.4, pp.993-1003, 2021.

[18] J. Gong and R. Xie, MPPT control by using a U-P curve for PMSG-based small wind turbines, *Journal of Energy Engineering*, vol.142, no.3, 04015030, 2016.

[19] C. Ghatri, M. Ouassaid, M. Labbadi and Y. Errami, Integral-type terminal sliding mode control approach for wind energy conversion system with uncertainties, *Comput. Electr. Eng.*, vol.99, 107775, 2022.

[20] H. K. Khalil, *Nonlinear Systems*, 2nd Edition, Prentice Hall, 1996.

Author Biography

Saleh Alshamali obtained his B.S. degree in Electrical and Computer Engineering in 1997 from the University of Missouri-Columbia, USA. He received the M.S. degree and the Ph.D. degree in Electrical Engineering in 2000 and 2004 from the University of Florida, Gainesville, USA.

Dr. Alshamali is currently an Associate Professor in the Electrical Engineering Department at Kuwait University. His research interests include the stability of nonlinear systems, the control design of linear and nonlinear systems, optimal control theory, and control applications.

Dana Alawadhi obtained her Bachelor of Science degree in Electrical Engineering in 2010 from the College of Engineering and Petroleum at Kuwait University. She received her Master's degree in Electrical Engineering in 2019 from the College of Graduate Studies at Kuwait University.

Ms. Alawadhi is currently working in the Engineering and Maintenance Department of the Public Authority for Applied Education and Training. Her research interests are linear and nonlinear control applications.

Elham Aljuwaiser acquired her B.S. degree and M.S. degree in Electrical Engineering in 2002 and 2006 from Kuwait University, Kuwait. She received her Ph.D. degree in Electronics and Electrical Communications Engineering in 2017 from Cairo University, Egypt.

Dr. Aljuwaiser is currently a teaching assistant in the Electrical Engineering Department at Kuwait University. Her research interests include nonlinear control systems, optimal control theory, state estimation, and stochastic filters.